https://doi.org/10.5194/egusphere-2022-888
Preprint. Discussion started: 7 September 2022

Short Communication: *age2exhume* - A Matlab script to calculate steady-state vertical exhumation rates from thermochronologic ages in regional datasets and application to the Himalaya

Peter van der Beek[1*], Taylor F. Schildgen[2,1*]

[1] Institute for Geosciences, University of Potsdam, Potsdam, Germany.

[2] GFZ German Research Centre for Geosciences, Potsdam Germany.

* Both authors contributed equally to this work.

Correspondence to: Peter van der Beek (vanderbeek@uni-potsdam.de)

Abstract.

Interpreting cooling ages from multiple thermochronometric systems and/or from steep elevation transects with the help of a thermal model can provide unique insights into the spatial and temporal patterns of rock exhumation. This information can, in turn, provide clues to the driving mechanisms of landscape evolution. Although several well-established thermal models allow for a detailed exploration of how cooling (and sometimes exhumation) rates evolved in a limited area or along a transect, information from large, regional datasets has been largely underutilized. Here, we present age2exhume, a thermal model in the form of a Matlab script, which can be used to rapidly provide a synoptic overview of exhumation rates from large, regional thermochronologic datasets. The model incorporates surface temperature based on a defined lapse rate and a local relief correction that is dependent on the thermochronometric system of interest. Other inputs include sample cooling age, uncertainty, thermochronometric system, and an initial (unperturbed) geothermal gradient. The model is simplified in that it assumes steady, vertical rock-uplift and unchanging topography when calculating exhumation rates. For this reason, it does not replace more powerful and versatile thermal-kinematic models, but it has the advantage of simple implementation and rapidly calculated results. In our example dataset, we show exhumation rates calculated from 1785 cooling ages from the Himalaya associated with five different thermochronometric systems. Despite the synoptic nature of the results, we show how they reflect known segmentation patterns and changing exhumation rates in areas that have undergone structural reorganization. Moreover, the rapidly calculated results enable an exploration of the sensitivity of the results to various input parameters, and an illustration of the importance of explicit modelling of thermal fields when calculating exhumation rates from thermochronologic data.

https://doi.org/10.5194/egusphere-2022-888
Preprint. Discussion started: 7 September 2022

1. Introduction

The steady accumulation of published thermochronologic data from around the world provides an opportunity to constrain spatial patterns of long-term (million-year timescale) exhumation with high granularity over vast swaths of the Earth's surface. This information can, in turn, provide clues to the driving mechanisms of orogen development and landscape evolution. Several well-established thermal models can be used to extract detailed cooling histories (and sometimes exhumation rates) from input cooling ages spread over a limited area or along an elevation transect. However, information from large datasets, comprising cooling ages from multiple thermochronometers spread over a wide region, has been largely underutilized due to the lack of easy-to-use tools that will handle vast, multi-system datasets.

The most advanced modeling tools in common use by the thermochronologic community include Pecube (Braun et al., 2012), HeFTy (Ketcham, 2005), QTQt (Gallagher, 2012), and GLIDE (Fox et al., 2014). Pecube is unique in its ability to handle forward and inverse thermal-kinematic modeling of spatially distributed data, including the options for time-varying topography and spatially and temporally variable rock-uplift patterns driven by defined fault geometries and kinematics. This complexity, however, entails substantial set-up requirements and relatively high computational demands, which tend to limit the spatial extent of modeled datasets. HeFTy and QTQt, in contrast, model thermal histories only, for individual samples or samples that are assumed to fall into a pseudo-vertical alignment. GLIDE (Fox et al., 2014) was developed with the aim of extracting exhumation histories from regional datasets. While powerful, the temporally and spatially continuous coverage of calculated exhumation rates that the model produces requires interpolations that can be challenging to interpret without careful consideration of the spatial and temporal distribution of the input data (Fox et al., 2014; Schildgen et al., 2018).

Here we present a simple thermal model, age2exhume, which is optimized to provide a synoptic overview of exhumation rates from large regional datasets. This model, inspired by the original age2edot code (Brandon et al., 1998), takes the form of a Matlab script that solves for steady-state exhumation rates from input thermochronologic ages, assuming vertical exhumation pathways and unchanging topography. A key difference between age2edot and age2exhume is that the former (despite its name) solves for ages given input exhumation rates, whereas our new model solves for exhumation rates given input ages. This difference makes age2exhume more suitable for calculating exhumation rates from regional datasets, since individual sample characteristics (e.g., an elevation-dependent surface temperature and local relief correction), included together with age in an input file, can be used to calculate an exhumation rate for each sample. A preliminary version of this code was used to visualize regional thermochronologic datasets in Schildgen et al. (2018); here, we provide more detailed background to the model and incorporate the individual sample characteristics mentioned above.

The regional (constant) inputs to the model include: (1) crustal thermal properties that can be approximated or derived from the literature (an initial, unperturbed geothermal gradient, thermal model thickness, and thermal diffusivity); and (2) kinetic parameters for the relevant thermochronometric system. Sample-specific inputs include (1) a local relief factor that can be extracted using standard GIS functions from a digital elevation model; and (2) sample properties (elevation, thermochronologic system, age, uncertainty). From our example dataset of 1785 cooling ages derived from five different thermochronologic

https://doi.org/10.5194/egusphere-2022-888
Preprint. Discussion started: 7 September 2022

systems in the Himalaya, steady-state, vertical exhumation rates with their uncertainties can be calculated within seconds on a standard laptop computer. Despite the synoptic nature of the results, we show how they reflect several fundamental features of the mountain belt, including strong regional differences that reflect known segmentation patterns and changing exhumation rates in areas that have undergone recent structural reorganization.

2. Background

2.1 Existing thermal models; their applications and limitations

Brandon et al. (1998) presented a simple, first-order approach to predict thermochronologic ages from input exhumation rates, in the form of a code called "age2edot". Age2edot calculates a steady-state conductive-advective geotherm and uses the approach of Dodson (1973) to predict the cooling-rate-dependent closure temperature of a given thermochronometric system. It then combines the predicted closure temperature and the steady-state geotherm to find the closure depth, and subsequently calculates a thermochronometric age by dividing the closure depth by the input exhumation rate. Kinetic parameters required for the Dodson (1973) calculation of closure temperature (see section 2.2 below) are derived from diffusion experiments for noble-gas based systems (i.e. (U-Th)/He and $^{40}Ar/^{39}Ar$) and from fitting an Arrhenius relation to experimental annealing data for fission-track systems (see Reiners and Brandon, 2006 for more detail). Simplifying assumptions in the age2edot approach include: (1) thermal steady state, (2) vertical exhumation paths, (3) unchanging topography, and (4) constant exhumation rates over the modelled time span. The most recent version of the age2edot code was released more than 15 years ago (Ehlers et al., 2005) and, because it was distributed as a Microsoft Windows executable, is now obsolete.

Willett and Brandon (2013) published a modification to the age2edot approach, in which the steady-state geotherm solution was replaced by an (inherently transient) half-space solution, a correction for the sample elevation with respect to the regionally averaged elevation was introduced, and a best-fit exhumation rate is predicted from an input age and a modern (i.e., final) geothermal gradient. The code was provided as a Matlab script. Although it is computationally efficient, two aspects of this model limit its use for modelling large regional datasets in our view; one is of a practical nature, whereas the other is more fundamental. The practical limitation lies in the need to provide a value (or bounding values) for the modern geotherm for each prediction. Although this requirement makes conceptual sense, since only the modern geotherm can potentially be measured, it is impractical when dealing with large datasets of widely varying ages because geothermal gradients are generally not known at more than very coarse spatial resolution, particularly in mountain belts, and they vary strongly in regions of variable exhumation rates. Starting from the modern geotherm also tends to make the code unstable, especially for very young thermochronological ages and corresponding high exhumation rates. The more fundamental problem lies in the choice of a thermal half-space model, which leads to a strong sensitivity of the geotherm to exhumation rate and the persistence of transient thermal conditions even after several tens of millions of years of steady exhumation (Willett and Brandon, 2013). One type of data that allows assessing if, and how rapidly, thermal steady state might be achieved in mountain belts is detrital thermochronology from sedimentary sequences in foreland basins. Several such datasets show constant lag times (i.e.,

https://doi.org/10.5194/egusphere-2022-888
Preprint. Discussion started: 7 September 2022

thermochronologic age minus depositional age), interpreted as recording establishment of thermal steady state in the source area after only a few million years, including in the western European Alps (Bernet et al., 2001, 2009), the central and eastern Himalaya (Bernet et al., 2006; Chirouze et al., 2013), the eastern Himalayan syntaxis (Bracciali et al., 2016; Lang et al., 2016; Govin et al., 2020), Taiwan (Kirstein et al., 2010) and the Southern Alps of New Zealand (Lang et al., 2020). As argued by Bracciali et al. (2016), modelling these constant lag times using a thermal half-space model would require *decreasing* exhumation rates through time, with a rate of decrease that exactly offsets the transient upward advection of the geotherm, in all the above cases. More probably, these data indicate that the thermal half-space model is not ideal for representing orogenic geotherms.

A completely different approach is taken by the thermal-history modelling codes HeFTy (Ketcham, 2005) and QTQt (Gallagher, 2012). These codes aim at predicting a thermal history from thermochronological ages and additional measurements (in particular fission-track length distributions, but also kinetic indicators) for single samples, although the most recent versions of these codes allow modelling suites of vertically offset samples. The output of these inverse models is an optimal time-temperature history and its uncertainty. These thermal history results require assumptions about the past geothermal gradient to be translated to a burial/exhumation history. Gallagher and Brown (1999) and Kohn et al. (2002) spatially interpolated thermal histories derived from large numbers of individual samples, using a precursor of the QTQt code, and combined them with heat-flow maps to derive regional to continental-scale images of denudation over geological time. This labor-intensive approach requires multiple thermochronologic systems and/or track-length data for each included sample in order to resolve meaningful thermal histories.

Pecube (Braun et al., 2012) is a three-dimensional thermal-kinematic code that predicts thermochronologic ages for various user-defined tectonic and geomorphic scenarios, taking into account the spatial and temporal perturbation of the geotherm by rock advection and transient topography. Pecube allows modelling both vertical and non-vertical exhumation paths, the latter controlled by a simple fault-kinematic model, and can be coupled to the natural-neighbor algorithm to run in inverse mode. The code has been used in a wide variety of tectonic and geomorphic settings (see Braun et al., 2012 for an overview), including at the scale of a small orogen (Curry et al., 2021). However, the fairly high computational demands of the code make it best suited for models of more limited spatial extent, where simple fault kinematics and/or spatially uniform rock-uplift can reasonably represent the tectonic deformation patterns.

GLIDE (Fox et al., 2014) comprises a linear inverse method to infer spatial and temporal variations in exhumation rate from spatially distributed low-temperature thermochronology datasets. The inversion assumes vertical exhumation and a smooth spatial variation in exhumation rates that can be described by a spatial correlation function. GLIDE uses the same thermal half-space model as the Willett and Brandon (2013) code, and the same caveats as to the appropriateness of this model thus apply. Moreover, it has been shown that the code translates abrupt spatial variations in thermochronological ages, such as across faults, into temporal increases in exhumation rates (Schildgen et al., 2018). Willett et al. (2021) argued that such issues occur mainly in areas of "insufficient" data coverage without, however, quantifying this term; Schildgen et al. (2018) showed that most sampled regions on Earth may have insufficient data coverage for unbiased prediction of exhumation-rate histories using

https://doi.org/10.5194/egusphere-2022-888
Preprint. Discussion started: 7 September 2022

GLIDE. Finally, as the GLIDE inversion depends on solving a large system of matrix equations, it does not run much faster than Pecube.

From the above abbreviated review, we conclude that a simple, first-order method to assess large regional datasets in a consistent manner is currently lacking from the thermochronology toolbox. We aim to provide such a simple method with the age2exhume code.

2.2 Age2exhume method

Fig. 1 shows a sketch outline and flowchart for the age2exhume model. When calculating exhumation rates from thermochronologic ages, a local relief correction (Δh) is needed to account for the difference in elevation of a sample (h) relative to an average-elevation (h_{avg}) surface that mimics the shape of the closure isotherm (Stüwe et al., 1994; Braun, 2002). We follow the procedure of Willett and Brandon (2013) in estimating the shape of the closure isotherm by averaging surface topography over a circle with a radius of $\pi \times z_c$, where z_c is an estimated closure depth for the relevant thermochronometric system. A brief guide for how to implement this correction using a Digital Elevation Model in ESRI ArcMap is provided in Appendix A. The local relief correction Δh is then calculated as:

$$\Delta h = h - h_{avg} \tag{1}$$

To predict a steady-state exhumation rate from thermochronologic age, surface temperature, and the local relief correction, the model starts with an initial guess of the closure depth (z_c) and exhumation rate ($\dot{e}$) from an initial, unperturbed linear geothermal gradient (G_{init}), a nominal closure temperature (T_c), and a surface temperature (T_s):

$$z_c = \frac{(T_c - T_s)}{G_{init}} \tag{2}$$

$$\dot{e} = \frac{z_c + \Delta h}{age} \tag{3}$$

T_s is estimated from an input sea-level temperature (T_0), the surface-temperature lapse rate (H), and the sample elevation (h): $T_{s(h)} = T_0 - H\,h$. The model then iteratively adapts T_c, z_c and $\dot{e}$ until convergence to a steady-state solution. At each iterative step, first the advective perturbation of the geotherm due to exhumation is calculated following Mancktelow and Grasemann (1997):

$$T_{(z)} = T_s + (T_L - T_s)\frac{(1 - e^{-z\dot{e}/\kappa})}{(1 - e^{-L\dot{e}/\kappa})} \tag{4}$$

where $T_{(z)}$ is the temperature at depth z, T_L is the temperature at the base ($z = L$) of the model ($T_L = T_s + G_{init}\,L$), and κ is the thermal diffusivity. Eq. (4) can be solved for the closure depth z_c:

$$z_c = z_{(T_c)} = \frac{\kappa}{\dot{e}} ln\left[1 - \frac{T_c - T_s}{T_L - T_s}\left(1 - e^{-L\dot{e}/\kappa}\right)\right] \tag{5}$$

Next, the closure temperature is re-estimated as a function of the cooling rate at the closure depth. First, the depth derivative of Eq. (4) is used to estimate the geothermal gradient:

$$\frac{dT}{dz} = \frac{\dot{e}(T_L - T_s)}{\kappa(1 - e^{-L\dot{e}/\kappa})} e^{-z\dot{e}/\kappa} \tag{6}$$

https://doi.org/10.5194/egusphere-2022-888
Preprint. Discussion started: 7 September 2022

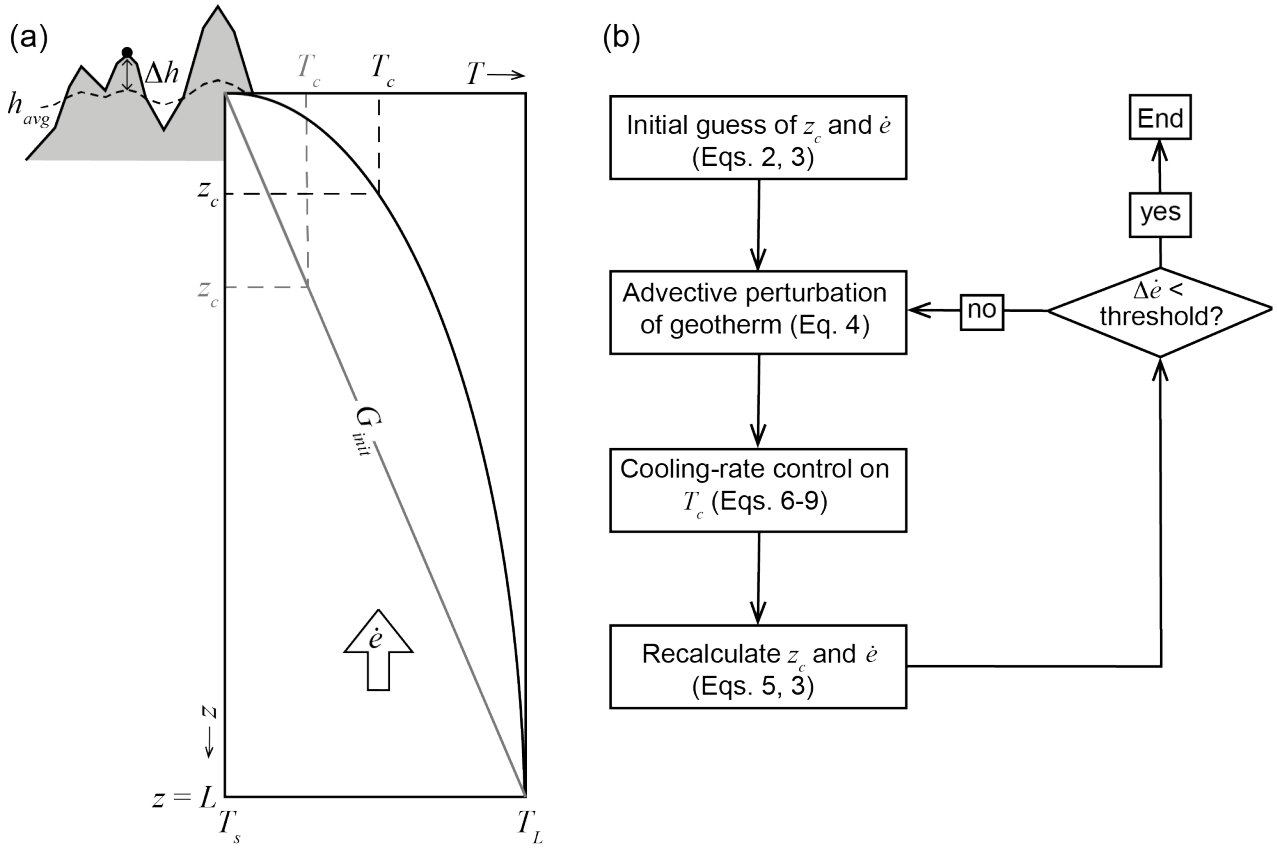

Figure 1: Model outline. (a) Sketch of model showing some of the main model parameters; main plot is a temperature – depth ($T-z$) plot of the model domain, showing initial linear geotherm and estimates of closure temperature (T_c) and closure depth (z_c) in grey, and final advectively perturbed geotherm and calculated T_c, z_c in black. Note that in most cases, T_c will increase because of the increased cooling rate (Eqs. 8, 9), while z_c will decrease due to the advective perturbation of the geotherm (Eq. 5). Inset shows how the local relief correction Δh is derived from the relationship between sample elevation (indicated by black dot) and average elevation h_{avg}. (b) Flow chart of the model and its main iteration loop.

Eq. (6) is evaluated at the closure depth z_c. Because $\dot{e} = dz/dt$, the cooling rate ($\dot{T}$) is:

$$\dot{T} = \frac{dT}{dt} = \frac{dT}{dz}\dot{e} \tag{7}$$

The model then uses the Dodson (1973) equation to relate closure temperature to cooling rate:

$$T_c = \frac{E_a}{R\, ln\left(A\tau\frac{D_0}{a^2}\right)} \tag{8}$$

where E_a (activation energy), D_0 (diffusivity at infinite temperature) and a (diffusion domain size) are experimentally determined kinetic parameters for each thermochronological system, A is a geometry factor and τ (characteristic time) is:

https://doi.org/10.5194/egusphere-2022-888
Preprint. Discussion started: 7 September 2022

$$\tau = -\frac{RT_c^2}{E_a \dot{T}} \quad (9)$$

Once a new estimate for T_c is obtained, z_c is updated using Eq. (5) and a new estimate for the exhumation rate is obtained with Eq. (3). The Matlab script steps through equations (3) – (9) iteratively (Fig. 1b) until the change in exhumation rate between successive steps ($\Delta\dot{e}$) is smaller than a threshold value; here we use $|\Delta\dot{e}/\dot{e}| < 10^{-3}$. To ensure smooth convergence, the exhumation rate used in each successive step is the average between the previous and the newly calculated rate.

Input parameters for the model include the kinematic parameters, the sea-level temperature T_0, atmospheric lapse rate H, the initial geothermal gradient G_{init}, thermal diffusivity κ, and model thickness L. The latter can represent the crustal thickness or, if more appropriate, the maximum depth from which rocks have been exhumed, such as the depth to a regional detachment horizon. Input data for each sample include a thermochronological age and its uncertainty at locations x and y, sample elevation h, and local relief correction Δh.

3. Results

3.1 General model predictions

Figs. 2 and 3 show contours of predicted exhumation rates for different combinations of age and Δh; Fig. 2 shows results for moderate exhumation rates (< 2 km Myr^{-1}) and thermochronologic ages up to 30 Ma, whereas Fig. 3 zooms in on the youngest ages (< 5 Ma) and shows results for exhumation rates up to 5 km Myr^{-1}. Input parameters for these models are as in Table 1, except that a constant surface temperature (T_s) of 10 °C was used, because absolute sample elevation is not included in these generic models. Kinetic parameters for the apatite (U-Th)/He (AHe) system are derived from Farley (2000); for the zircon (U-Th)/He (ZHe) system from Reiners et al. (2004); and for the apatite (AFT) and zircon (ZFT) fission-track systems from Reiners and Brandon (2006).

Parameter	Symbol	Value	Unit
Temperature at sea level	T_0	25	°C
Atmospheric lapse rate	H	5	°C km^{-1}
Initial geothermal gradient	G_{init}	25	°C km^{-1}
Thermal diffusivity	κ	30	km^2 Myr^{-1}
Model thickness	L	30	km

Table 1: input parameter values used in modelling Himalayan dataset

https://doi.org/10.5194/egusphere-2022-888
Preprint. Discussion started: 7 September 2022

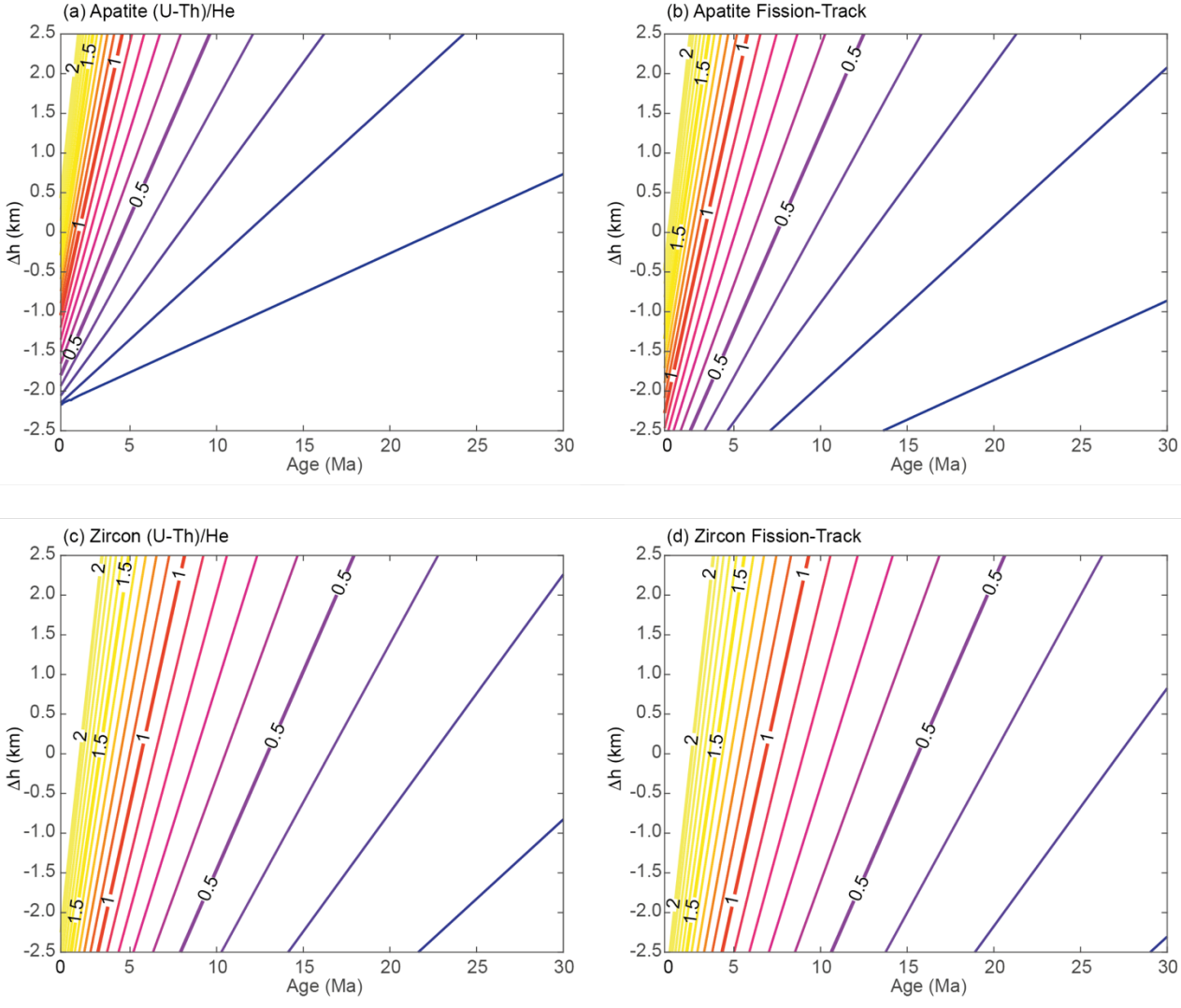

Figure 2: Contour plots of exhumation rate for different age – Δ*h* combinations. These can be thought of as age – elevation relationships for different constant exhumation rates. Plots are shown for the (a) AHe, (b) AFT, (c) ZHe, and (d) ZFT systems; exhumation-rate contours are shown every 0.1 km Myr^{-1} from 0.1 to 2.0 km Myr^{-1}.

https://doi.org/10.5194/egusphere-2022-888
Preprint. Discussion started: 7 September 2022

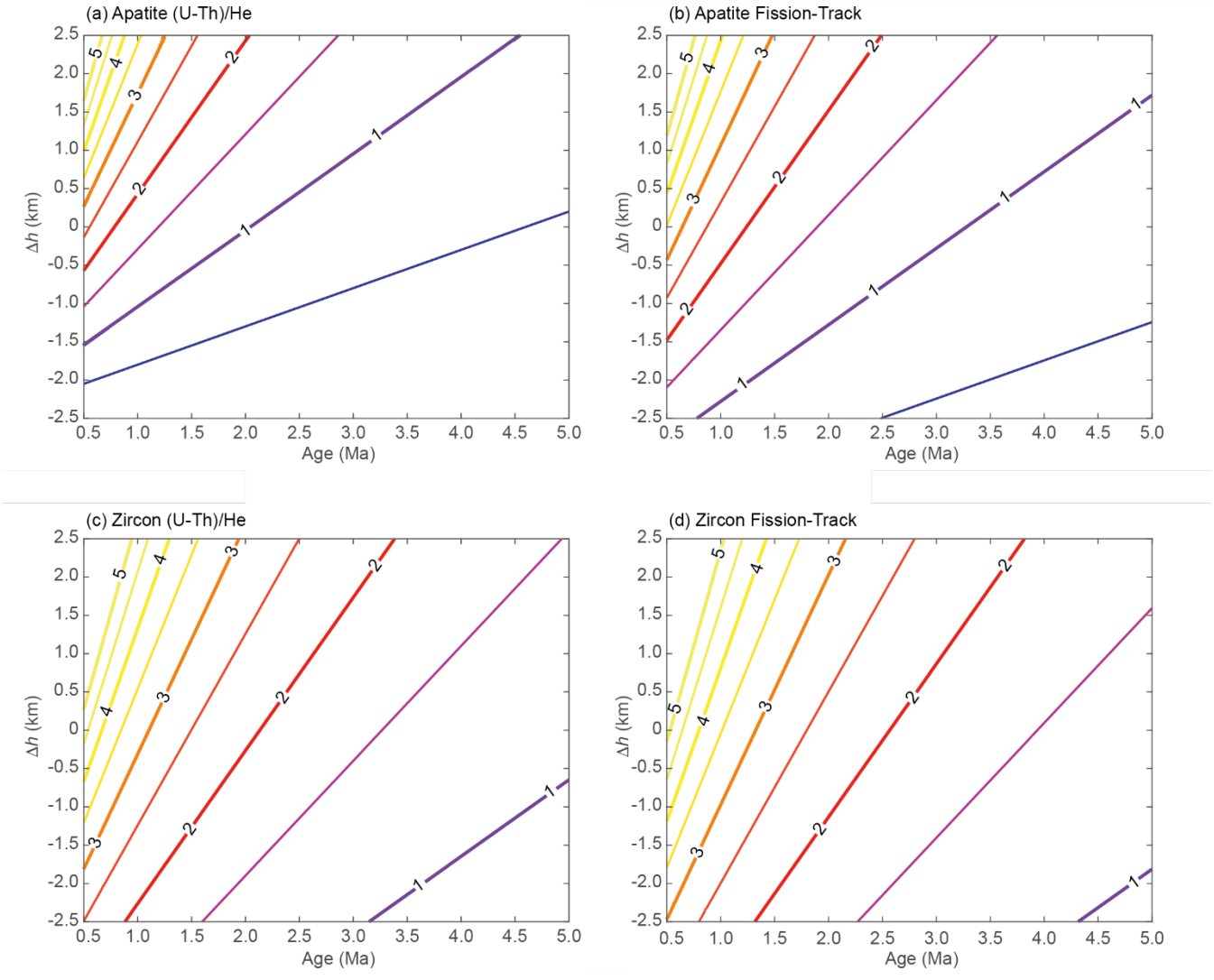

Figure 3: Contour plots of exhumation rate for different age – Δ*h* combinations, zooming in on rapid rates and young thermochronologic ages (< 5 Ma). Plots are shown for the (a) AHe, (b) AFT, (c) ZHe, and (d) ZFT systems; exhumation-rate contours are shown every 0.5 km Myr^{-1} from 0.5 to 5 km Myr^{-1}.

https://doi.org/10.5194/egusphere-2022-888
Preprint. Discussion started: 7 September 2022

These results can be thought of conceptually as showing age – elevation profiles for different constant exhumation rates, with elevation measured relative to an average regional elevation as defined in Section 2.2. They can also be used as a plotted lookup table for rapidly inferring exhumation rate from a given age, Δh combination.

3.2 Results from a Himalayan example data set

Our example data set from the Himalaya comprises 1785 thermochronologic ages compiled from papers published through July 2022; data sources are provided in the Supplementary Information. We have excluded some reported ages from the Siwaliks (Sub-Himalayan fold-thrust belt), as that sedimentary unit commonly yields unreset ages. We have also excluded the western and eastern syntaxis regions, where extremely rapid exhumation is driven by processes that are different from those in the main part of the Himalaya (Zeitler et al., 2014; Butler, 2019). Finally, we exclude any pre-Himalayan ages (> 60 Ma), as these are not directly linked to exhumation during Himalayan mountain building. Our data set comprises 345 white mica $^{40}Ar/^{39}Ar$ (MAr) ages, 236 ZFT ages, 783 AFT ages, 281 ZHe ages, and 140 AHe ages. All ages and sample details are included in a single input file in .txt format, with columns that include a sample ID number, latitude, longitude, elevation, Δh value, age, 1σ age uncertainty, and a numeric code for the thermochronologic system (Schildgen and van der Beek, 2022). Table 1 shows the parameters we assume for the surface temperature (T_0, H) and the thermal model (L, G_{init}, κ). Kinetic parameters used for the AHe, AFT, ZHe and ZFT systems are the same as for the general model predictions presented in section 2.1 above; we used the parameters from Hames and Bowring (1994) for the MAr system.

A map of the calculated exhumation rates for the Himalaya (Fig. 4), with exhumation plotted such that rates derived from lower-temperature systems plot on top of those from higher-temperature systems, reveals patterns in space and time that reflect well-known segmentation patterns of the range. In general, a band of rapid exhumation rates occurs at the topographic front of the high Himalaya, with slower rates recorded to the north and south. Within this band, the highest rates are generally recorded by the lower-temperature AHe and AFT thermochronometers, suggesting increasing exhumation rates with time. Note that such variable exhumation rates recorded by different co-located thermochronometers formally violate the assumption of constant exhumation rates through time made by the model. The rates inferred from the higher-temperature thermochronometers should therefore be considered rough estimates only; they will generally be overestimated in the case of increasing rates through time, and the corresponding rate change will therefore be underestimated. The focused rapid rates at the foot of the high Himalaya together with an increase in exhumation rates for lower-temperature systems is consistent with exhumation being driven by thrusting over a large-scale ramp in the Main Himalayan Thrust (MHT), the interface between the underthrusting Indian continent and the overlying Himalayan units, often associated with duplex development (e.g., Robert et al., 2009; Herman et al., 2010; Coutand et al., 2014; Dal Zilio et al., 2021; see van der Beek et al., in press and references therein for detailed discussions).

The highest exhumation rates (> 2 km Myr^{-1}) outside of the Himalayan syntaxes occur in central Nepal (~84 °E), Sikkim (~88 °E), the Kumaun Himalaya (~80 °E), and the Sutlej valley (~78 °E). High rates (between 1 and 2 km Myr^{-1}) are recorded along the high Himalayan front throughout northwest India (~76-80 °E) and more sporadically in eastern Nepal (~87 °E) and

https://doi.org/10.5194/egusphere-2022-888
Preprint. Discussion started: 7 September 2022

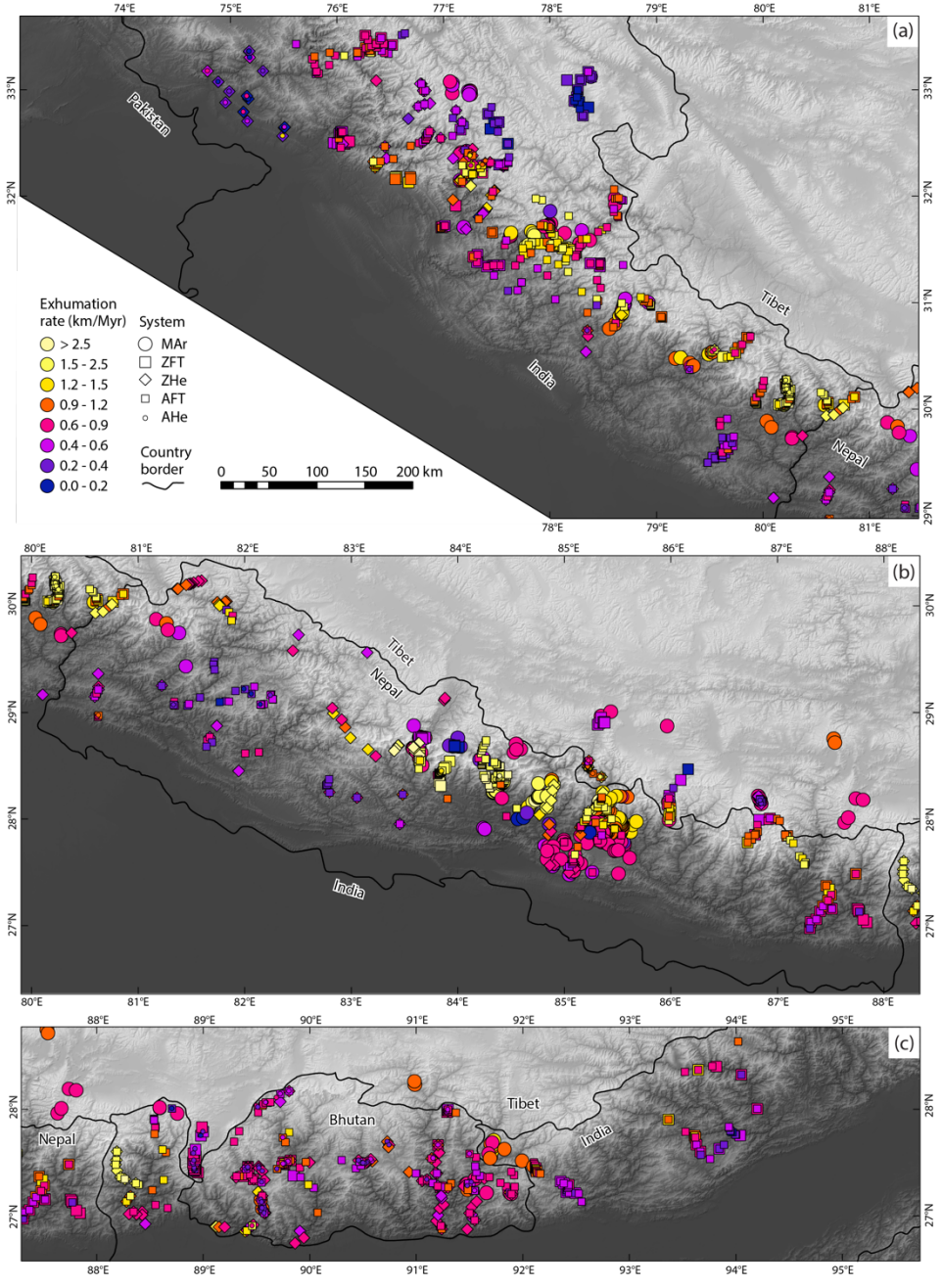

Figure 4: Exhumation rates inferred from Himalayan dataset of 1785 thermochronologic ages. (a) western Himalaya (Kashmir to Nepal); (b) Nepal Himalaya; (c) eastern Himalaya (Sikkim to Arunachal Pradesh). Data points are coloured by exhumation rate; symbols indicate different thermochronometric systems (see legend in (a)).

https://doi.org/10.5194/egusphere-2022-888
Preprint. Discussion started: 7 September 2022

western Bhutan (~89 °E). The lowest exhumation rates along the high Himalayan topographic front (< 0.8 km Myr^{-1}) are found in Kashmir (west of ~75 °E), western Nepal (~81 °E), and from western Bhutan (~90 °E) to the east. These lateral variations in exhumation rates have been interpreted as reflecting lateral variations in the presence/absence and geometry (location, height and dip) of the mid-crustal ramp in the MHT, together with duplex formation and local out-of-sequence thrusting (Hubbard et al., 2021; Dal Zilio et al., 2021; van der Beek et al., in press). In some of the more slowly exhuming regions, in particular in Bhutan, exhumation rates appear to be decreasing through time, with lower-temperature systems recording lower exhumation rates than higher-temperature systems. Decreasing exhumation rates in Bhutan can be linked to slowing convergence across the Bhutan Himalaya due to transfer of deformation to the Shillong Plateau to the south (Clark and Bilham, 2008; Coutand et al., 2014, 2016). Similar to the caveats described above concerning increasing exhumation rates, in areas of decreasing exhumation rates, the change in rates through time recorded by different systems will also be underestimated.

The above example illustrates how this method can rapidly obtain internally consistent estimates of exhumation rates from multiple thermochronometers from different elevations over a large region. Inferred patterns of exhumation rates can be linked to structural and geophysical observations of orogen segmentation, as above, or to orogen-wide topographic measures for assessing first-order linkages between exhumation rates and morphology (e.g., Clubb et al., *Himalayan valley width controlled by tectonics rather than discharge*; manuscript in preparation). This rapid analysis can also highlight areas where rates appear to be temporally changing, and thus the basic assumptions of the model break down. More detailed regional explorations of the kinematics and controls on exhumation rates can then be applied to such subsets of the data (e.g., van der Beek et al, in press and references therein).

4. Discussion and Conclusions

4.1 Importance, uncertainties and sensitivity

An advantage of the rapid calculations performed by age2exhume is that it is easy to explore the sensitivity of the calculated exhumation rates to different input parameters (i.e., sample-specific information and crustal/thermal properties), in addition to evaluating how the iterative method compares to simpler estimates of exhumation rates. Regarding the latter, we can compare calculated exhumation rates from age2exhume to those that would be obtained by assuming a simple linear geotherm and fixed nominal closure temperature, T_c. Fig. 5a compares "initial" exhumation rates, calculated using Eqs. 2 and 3 (hence, a linear geotherm and fixed T_c), with the final exhumation rates predicted by age2exhume, which incorporate perturbations to the geotherm and T_c. Initial exhumation rates are calculated using the same thermal parameters of Table 1 and nominal closure temperatures of 70 °C for the AHe system, 120 °C for the AFT system, 180 °C for the ZHe system, 220 °C for the ZFT system, and 350 °C for the MAr system. The comparison shows that for exhumation rates up to ~0.5 km Myr^{-1}, there is little difference between the two methods (Fig. 5a). At higher exhumation rates, the methods deviate substantially, with the initial estimate systematically overestimating the exhumation rate. For example, at exhumation rates ≥2 km Myr^{-1}, overestimates mostly fall

https://doi.org/10.5194/egusphere-2022-888
Preprint. Discussion started: 7 September 2022

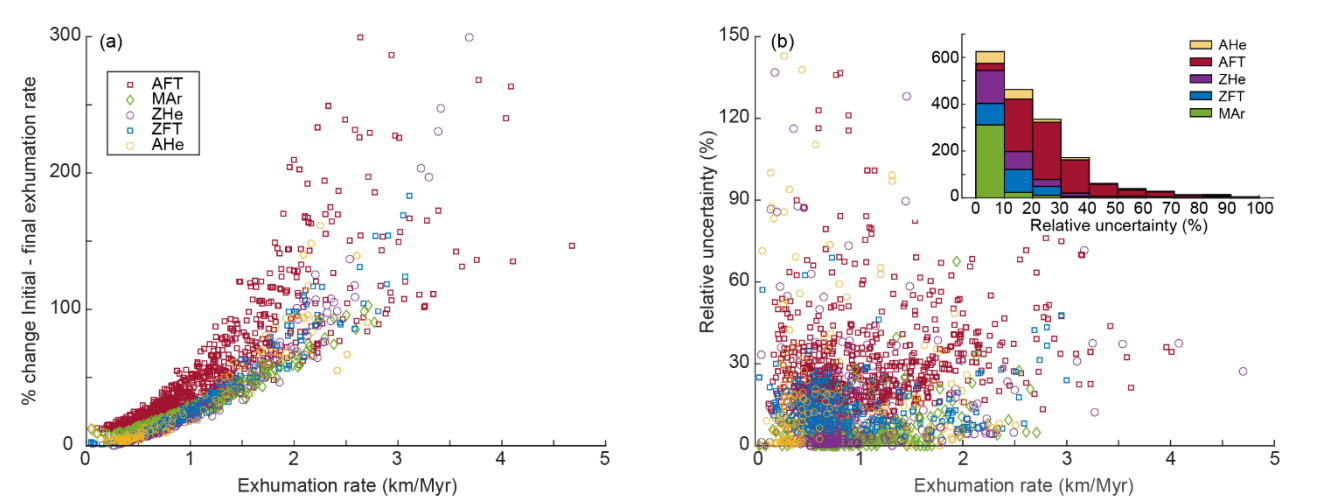

Figure 5: Impact of including perturbations to the geotherm and T_c in estimates of exhumation rate, and uncertainties in exhumation-rate calculations. (a) Comparison of initial exhumation rate ($\dot{e}_{init}$; assuming a linear geothermal gradient and nominal closure temperatures) for the Himalayan data against final exhumation rate ($\dot{e}$), calculated using the age2exhume method. The impact is expressed as a percent change between the two results; i.e., $100 \times (\dot{e}_{init} - \dot{e})/\dot{e}$. Symbols indicate different thermochronometric systems. (b) Relative uncertainty in exhumation rate calculated by propagating uncertainty in age. Symbols are as in (a). Inset shows stacked histograms of relative uncertainty for different systems. See text for discussion.

between 100 and 300%. These findings can be explained by considering the relative importance of two competing influences on the closure depth z_c (Fig. 1a), which directly determines the exhumation rate (Eq. 3). On one hand, higher cooling rates – linked to higher exhumation rates – lead to an increase in T_c, and hence a deepening of z_c (Eqs. 8, 9). On the other hand, the advective perturbation of the geotherm due to exhumation, which forces an upward deflection of isotherms, leads to a shallowing of z_c for any T_c (Eq. 5). The degree of advective perturbation of the geotherm is characterized by the non-dimensional Péclet number: $Pe = \dot{e}\, L/\kappa$ (e.g., Braun et al., 2006). With higher exhumation rates, the effect of upward, advective perturbation of isotherms on z_c dominates over the effect of the increasing T_c on z_c. The scatter in the amount of overestimation, in particular for the lower-temperature AFT and AHe systems, is linked to the effect of including Δh, which is more important for shallower z_c (Eq. 3).

But how important are these differences in the method of calculating exhumation rates relative to the uncertainties in any calculated rate? The uncertainties in reported ages are just one component of the total uncertainty that one can consider in an exhumation-rate calculation, but the direct propagation of age uncertainty into the uncertainty on an inferred exhumation rate provides a simple means of comparison (Fig. 5b). Because of the non-linear relationship between age and exhumation rate, the

https://doi.org/10.5194/egusphere-2022-888
Preprint. Discussion started: 7 September 2022

uncertainties in exhumation rates are asymmetric, with $\dot{e}_{max} - \dot{e} > \dot{e} - \dot{e}_{min}$. The bulk of the relative uncertainties in exhumation rates associated with age uncertainty lie between 10 and 50%, and they are not strongly dependent on exhumation rate. Higher-temperature systems (ZHe, ZFT and MAr) are generally associated with lower exhumation-rate uncertainties (< 10%) because of the smaller age uncertainties associated with these systems. In contrast, AFT data can have very large associated uncertainties of up to >100%, because low track counts due to low U-contents and/or young ages yield large age uncertainties. Some large relative uncertainties in the AHe and ZHe systems at lower exhumation rates (< 1 km Myr^{-1}) are probably associated with larger inter-grain scatter in ages due to compositional and grainsize effects that become more important at lower cooling and exhumation rates (e.g., Whipp et al., 2022 and references therein). Overall, however, the bulk of the uncertainties in exhumation rate are smaller than the differences between the initial and final exhumation rates shown in Fig. 5a for exhumation rates > ~0.5 km Myr^{-1}. This comparison implies that the thermal effects of exhumation significantly affect inferred exhumation rates.

The importance of including sample-specific information in exhumation-rate calculations is illustrated in Figs. 6a and 6b. Our comparison of exhumation rates calculated with a constant surface temperature, T_s, versus those calculated with T_s dependent on elevation shows a relatively small effect, with differences mostly less than 10%. However, for the low-temperature thermochronometers AHe and AFT at exhumation rates < 1 km Myr^{-1}, differences can reach 20% (Fig. 6a). The effect of the local relief correction, Δh, for each sample is generally more important. Although the magnitude of Δh tends to be reduced for the lower-temperature systems (because their closure isotherms more closely mimic surface topography), any given Δh has a stronger impact on exhumation rates for low-temperature systems compared to high-temperature systems (Fig. 6b). Moreover, the effects are asymmetric: negative Δh values lead to a larger correction in exhumation rates compared to positive Δh values. For example, a Δh of +1 km will lead to a ca. 20% change in calculated exhumation rate for the AFT system, whereas a Δh of -1 km will lead to a 30 to 50% change (Fig. 6b). The importance of including Δh when calculating exhumation rates is further emphasized considering that samples are more commonly collected from valley bottoms (with negative Δh values) than ridgetops. Our Himalayan example dataset bears this out: the histogram of Δh values is strongly skewed toward negative values, with a median Δh of -0.53 km (Fig. 6b inset).

We next explore the sensitivity of calculated exhumation rates to crustal parameters, including the initial geothermal gradient G_{init} (Fig. 6c), and model thickness L (Fig. 6d). These plots show the percent change in predicted exhumation rates when changing these two parameters to either a higher or a lower value. Decreasing L from 30 to 20 km leads to higher predicted exhumation rates (by up to ~ 40 %), whereas increasing L from 30 to 40 km leads to lower predicted exhumation rates (by up to ~ -20 %), with the magnitude of the effect increasing with exhumation rate. This behavior can be understood by considering the effect L has on the advective perturbation of the geotherm, through the Péclet number (see above). The sensitivity of the predictions to G_{init} is of similar magnitude when considering changes from 25 to 30 °C/km or from 25 to 20 °C/km (Fig. 6c), but in this case, the effect is strongest for relatively low exhumation rates. For both L and G_{init}, predictions based on higher-temperature thermochronometers (ZFT and MAr) are slightly more sensitive to the input thermal parameters than the lower-temperature systems (AHe and AFT).

https://doi.org/10.5194/egusphere-2022-888
Preprint. Discussion started: 7 September 2022

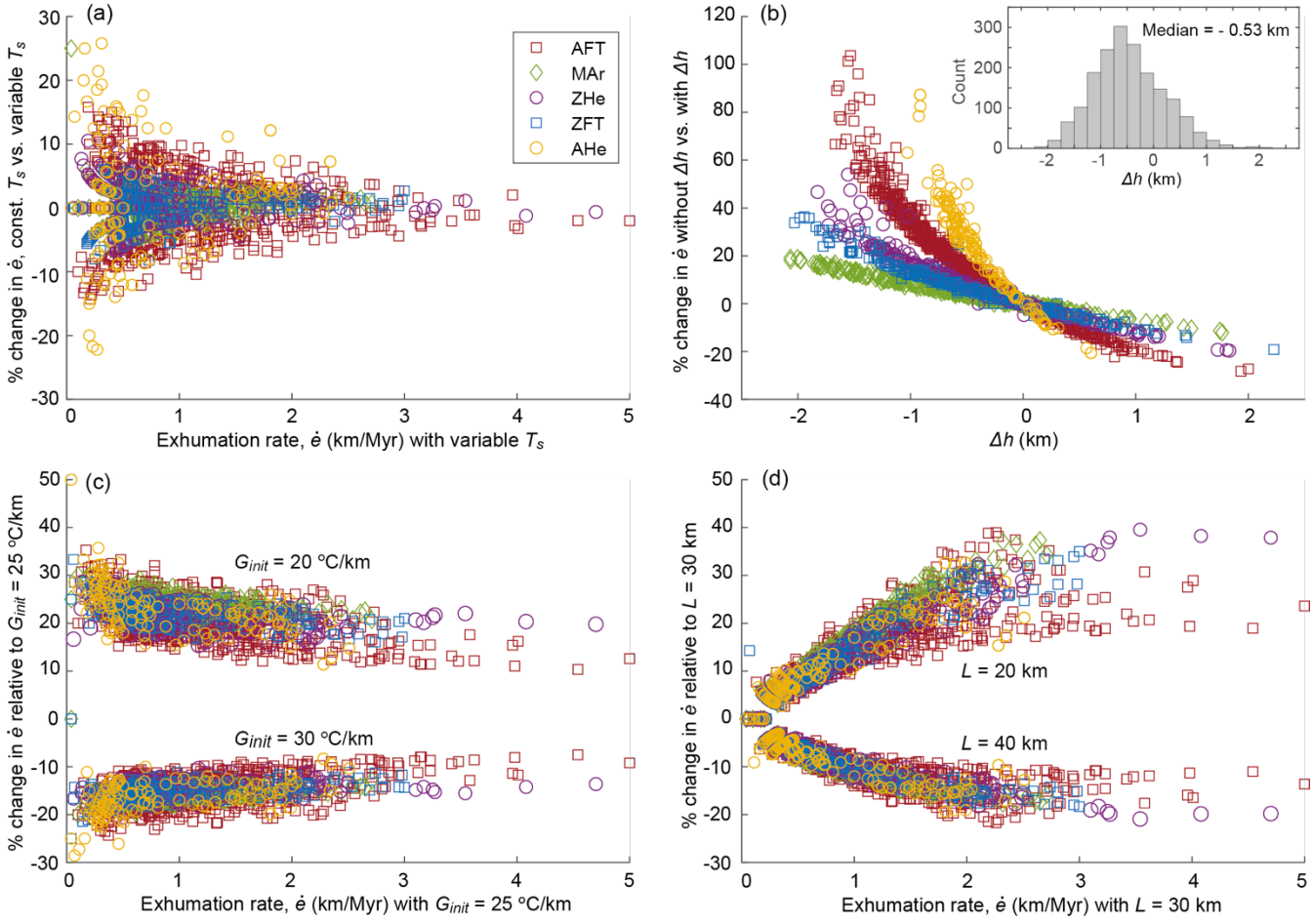

Figure 6: Impact of varying surface conditions and sensitivity to thermal parameters on calculated exhumation rates. (a) Impact of using a variable (elevation-dependent) surface temperature versus a constant surface temperature; (b) impact of including the local relief correction Δh; inset shows histogram of Δh values for the Himalayan dataset; (c) sensitivity of predicted exhumation rates to initial geothermal gradient G_{init}; (d) sensitivity of predicted exhumation rates to model thickness L. Plots show percent change in exhumation rates for varying conditions versus exhumation rate predicted with parameters of Table 1; i.e., 100 x (tested change – default value)/default value, where "default value" is defined as in Table 1. See text for discussion.

4.2 Concluding remarks

The model presented here allows obtaining a rapid, first-order, synoptic view of spatial and temporal variations in exhumation rates, calculated in a self-consistent manner from different thermochronometers over a large region. We provide three different versions of the code on Zenodo (van der Beek and Schildgen, 2022): (1) a basic version that takes a single age – Δh pair as

https://doi.org/10.5194/egusphere-2022-888
Preprint. Discussion started: 7 September 2022

input and returns a single exhumation rate; (2) a version for which a range of thermochronologic ages and Δh values are provided and that returns a lookup table of exhumation rates (used in Section 3.1 and Figs. 2, 3); and (3) a version that reads an input file of sample locations, elevation, thermochronologic system, age and uncertainty, and returns a table of exhumation rates with uncertainty for each sample (used in section 3.2 and Fig. 4). We anticipate the latter version to be most useful but include the other two for completeness.

The main advantage of our approach over the version of age2edot presented by Willett and Brandon (2013) is that our model does not require the final geothermal gradient as input, but only the initial, unperturbed geotherm. This aspect of our model makes it easily applicable to regions with variable exhumation rates, which are expected to have a wide range of modern geothermal gradients. Also, our model assumption of a constant basal temperature, although obviously a significant simplification, appears to provide a more reasonable approximation to the thermal structure of mountain belts than the thermal half-space solution implemented in Willett and Brandon (2013).

Our model has important limitations: it assumes steady-state exhumation, unchanging topography, and vertical exhumation pathways, so it is only appropriate for obtaining first-order, synoptic overviews of exhumation-rate patterns. Nevertheless, in the case where ages from multiple thermochronometers are available from individual samples or from samples in close proximity to one another, differences in exhumation rates derived from those ages can be used to map out where changes in exhumation rates have likely occurred, and thus highlight regions where more detailed thermal modeling could be used to extract non-steady-state exhumation histories. In cases where this method indicates non-steady exhumation, the predicted differences in rates between high- and low-temperature thermochronometers are likely to underestimate the real change in exhumation rate that has occurred.

The model assumptions of a constant basal temperature together with an input model thickness are unlikely to be valid over long timescales, and in many cases can only be estimated roughly. However, the speed with which exhumation rates can be calculated from our model enables users to easily investigate the sensitivity of their results to these estimated values. Moreover, while these thermal parameters change the absolute values of the predicted exhumation rates, they affect all predictions similarly (if not equally). Therefore, their influence on spatial patterns in exhumation rates or the correlation of exhumation rates with other metrics will be limited.

Appendix A: Calculating Δh from digital elevation datasets

To calculate Δh, Willett and Brandon (2013) suggest calculating a mean value for a circle that has a radius equal to $\pi \times z_c$, where z_c is the closure depth of the system. This operation can be done with standard operations in a geographic information system (GIS), or other tools designed to work with continuous raster datasets.

In ESRI's ArcMap version 10.8.1, the mean elevation can be calculated using the Focal Statistic function, found within the "Spatial Analyst Tools - Neighborhood" tools in Arc Toolbox. The Focal Statistic function provides an option to average values over a moving circular window with a radius defined by map units or by a number of pixels. For example, for a standard

https://doi.org/10.5194/egusphere-2022-888
Preprint. Discussion started: 7 September 2022

90-m resolution SRTM DEM, and for a desired z_c of 2000 m (e.g., for the AHe system), the radius of the circle should be 6280 m, which is approximately equivalent to 70 pixels.

To rapidly calculate Δh for all samples in a large dataset, it is practical to take advantage of the "Raster Calculator" (Spatial Analyst Tools – Map Algebra) and the "Extract Values to Points" functions (Spatial Analyst Tools – Extraction). The Map Calculator can be used to subtract the smoothed DEM from the previous step from the modern SRTM DEM. This operation will produce a continuous raster data set of Δh values. The "Extract Values to Points" function samples a raster at the position of each sample data point, and adds the extracted value to a new column ("field") in the attribute table of the shapefile.

If elevations are not included in a regional dataset, or if the user-reported elevations may be unreliable (e.g., based on readings from hand-held GPS units), the same function can be used to extract elevation values from the SRTM DEM and added to the attribute table. However, if the "Extract" function is used more than once to add new fields to an attribute table, it may be necessary to copy the first set of values into a manually created field, as some versions of ArcMap do not readily permit renaming (or overwriting) of the field obtained from the first "Extract" operation. Although the exact procedure described here may differ for other versions of ArcMap, general functions to calculate focal statistics, perform arithmetic operations on raster datasets, and automated extraction of values from rasters at the location of sample points can be found in many versions of the software.

Code Availability. The Matlab scripts for three versions of the age2exhume code are included in the Zenodo repository: age2exhume Matlab scripts (https://doi.org/10.5281/zenodo.7053218).

Data Availability. Data used in the example data set was compiled from the sources listed in the Supplementary Material. A text file containing the full dataset is included in the Zenodo repository: Thermochronology dataset for Himalaya (https://doi.org/10.5281/zenodo.7053115).

Author Contributions. Both authors contributed equally to the development of the code, the compilation of the Himalayan dataset, sensitivity analyses, and writing of the manuscript.

Competing Interests. The authors declare no competing interests.

Acknowledgements. T.S. acknowledges support from the ERC Consolidator Grant #863490 GyroSCoPe; P.v.d.B. acknowledges support from the ERC Advanced Grant #834271 COOLER.

https://doi.org/10.5194/egusphere-2022-888
Preprint. Discussion started: 7 September 2022

References

Bernet, M., Zattin, M., Garver, J. I., Brandon, M. T., and Vance, J. A.: Steady-state exhumation of the European Alps, Geology, 29, 35–38, https://doi.org/10.1130/0091-7613(2001)029<0035:sseote>2.0.co;2, 2001.

Bernet, M., van der Beek, P., Pik, R., Huyghe, P., Mugnier, J.-L., Labrin, E., and Szulc, A.: Miocene to Recent exhumation of the central Himalaya determined from combined detrital zircon fission-track and U/Pb analysis of Siwalik sediments, western Nepal, Basin Res., 18, 393–412, https://doi.org/10.1111/j.1365-2117.2006.00303.x, 2006.

Bernet, M., Brandon, M., Garver, J., Balestrieri, M. L., Ventura, B., and Zattin, M.: Exhuming the Alps through time: clues from detrital zircon fission-track thermochronology, Basin Res., 21, 781–798, https://doi.org/10.1111/j.1365-2117.2009.00400.x, 2009.

Bracciali, L., Parrish, R. R., Najman, Y., Smye, A., Carter, A., and Wijbrans, J. R.: Plio-Pleistocene exhumation of the eastern Himalayan syntaxis and its domal 'pop-up,' Earth Sci. Rev., 160, 350–385, https://doi.org/10.1016/j.earscirev.2016.07.010, 2016.

Brandon, M. T., Roden-Tice, M. K., and Garver, J. I.: Late Cenozoic exhumation of the Cascadia accretionary wedge in the Olympic Mountains, northwest Washington State, Geol. Soc. Am. Bull., 110, 985–1009, https://doi.org/10.1130/0016-7606(1998)110<0985:lceotc>2.3.co;2, 1998.

Braun, J.: Quantifying the effect of recent relief changes on age–elevation relationships, Earth Planet. Sci. Lett., 200, 331–343, https://doi.org/10.1016/s0012-821x(02)00638-6, 2002.

Braun, J., van der Beek, P., and Batt, G. E.: Quantitative Thermochronology: Numerical methods for the interpretation of thermochronological data, Cambridge University Press, 271 pp., 2006.

Braun, J., van der Beek, P., Valla, P., Robert, X., Herman, F., Glotzbach, C., Pedersen, V., Perry, C., Simon-Labric, T., and Prigent, C.: Quantifying rates of landscape evolution and tectonic processes by thermochronology and numerical modeling of crustal heat transport using PECUBE, Tectonophysics, 524–525, 1–28, https://doi.org/10.1016/j.tecto.2011.12.035, 2012.

Butler, R. W. H.: Tectonic evolution of the Himalayan syntaxes: the view from Nanga Parbat, Geol. Soc. London Spec. Publ., 483, 215–254, https://doi.org/10.1144/sp483.5, 2019.

Chirouze, F., Huyghe, P., van der Beek, P., Chauvel, C., Chakraborty, T., Dupont-Nivet, G., and Bernet, M.: Tectonics, exhumation, and drainage evolution of the eastern Himalaya since 13 Ma from detrital geochemistry and thermochronology, Kameng River Section, Arunachal Pradesh, Geol. Soc. Am. Bull., 125, 523–538, https://doi.org/10.1130/b30697.1, 2013.

Clark, M. K. and Bilham, R.: Miocene rise of the Shillong Plateau and the beginning of the end for the Eastern Himalaya, Earth Planet. Sci. Lett., 269, 336–350, https://doi.org/10.1016/j.epsl.2008.01.045, 2008.

Coutand, I., Whipp, D. M., Grujic, D., Bernet, M., Fellin, M. G., Bookhagen, B., Landry, K. R., Ghalley, S. K., and Duncan, C.: Geometry and kinematics of the Main Himalayan Thrust and Neogene crustal exhumation in the Bhutanese Himalaya derived from inversion of multithermochronologic data, J. Geophys. Res., 119, 1446–1481, https://doi.org/10.1002/2013jb010891, 2014.

Coutand, I., Barrier, L., Govin, G., Grujic, D., Hoorn, C., Dupont-Nivet, G., and Najman, Y.: Late Miocene-Pleistocene evolution of India-Eurasia convergence partitioning between the Bhutan Himalaya and the Shillong Plateau: New evidences from foreland basin deposits along the Dungsam Chu section, eastern Bhutan, Tectonics, 35, 2963–2994, https://doi.org/10.1002/2016tc004258, 2016.

Curry, M. E., van der Beek, P., Huismans, R. S., Wolf, S. G., Fillon, C., and Muñoz, J.-A.: Spatio-temporal patterns of Pyrenean exhumation revealed by inverse thermo-kinematic modeling of a large thermochronologic data set, Geology, 49, 738–742, https://doi.org/10.1130/g48687.1, 2021.

https://doi.org/10.5194/egusphere-2022-888
Preprint. Discussion started: 7 September 2022

Dal Zilio, L., Hetényi, G., Hubbard, J., and Bollinger, L.: Building the Himalaya from tectonic to earthquake scales, Nat. Rev. Earth Environ., 2, 251–268, https://doi.org/10.1038/s43017-021-00143-1, 2021.

Dodson, M. H.: Closure temperature in cooling geochronological and petrological systems, Contrib. Mineral. Petrol., 40, 259–274, https://doi.org/10.1007/bf00373790, 1973.

Ehlers, T. A., Chaudhri, T., Kumar, S., Fuller, C. W., Willett, S. D., Ketcham, R. A., Brandon, M. T., Belton, D. X., Kohn, B. P., Gleadow, A. J. W., Dunai, T. J., and Fu, F. Q.: Computational tools for low-temperature thermochronometer interpretation, Rev. Mineral. Geochem., 58, 589–622, https://doi.org/10.2138/rmg.2005.58.22, 2005.

Farley, K. A.: Helium diffusion from apatite: General behavior as illustrated by Durango fluorapatite, J. Geophys. Res., 105, 2903–2914, https://doi.org/10.1029/1999jb900348, 2000.

Fox, M., Herman, F., Willett, S. D., and May, D. A.: A linear inversion method to infer exhumation rates in space and time from thermochronometric data, Earth Surf. Dyn., 2, 47–65, https://doi.org/10.5194/esurf-2-47-2014, 2014.

Gallagher, K.: Transdimensional inverse thermal history modeling for quantitative thermochronology, J. Geophys. Res., 117, B02408, https://doi.org/10.1029/2011jb008825, 2012.

Gallagher, K. and Brown, R.: The Mesozoic denudation history of the Atlantic margins of southern Africa and southeast Brazil and the relationship to offshore sedimentation, Geol. Soc. London, Spec. Publ., 153, 41–53, https://doi.org/10.1144/gsl.sp.1999.153.01.03, 1999.

Govin, G., van der Beek, P., Najman, Y., Millar, I., Gemignani, L., Huyghe, P., Dupont-Nivet, G., Bernet, M., Mark, C., and Wijbrans, J.: Early onset and late acceleration of rapid exhumation in the Namche Barwa syntaxis, eastern Himalaya, Geology, 48, 1139–1143, https://doi.org/10.1130/g47720.1, 2020.

Hames, W. E. and Bowring, S. A.: An empirical evaluation of the argon diffusion geometry in muscovite, Earth Planet. Sci. Lett., 124, 161–169, https://doi.org/10.1016/0012-821x(94)00079-4, 1994.

Herman, F., Copeland, P., Avouac, J.-P., Bollinger, L., Mahéo, G., Fort, P. L., Rai, S., Foster, D., Pêcher, A., Stüwe, K., and Henry, P.: Exhumation, crustal deformation, and thermal structure of the Nepal Himalaya derived from the inversion of thermochronological and thermobarometric data and modeling of the topography, J. Geophys. Res., 115, B06407, https://doi.org/10.1029/2008jb006126, 2010.

Hubbard, M., Mukul, M., Gajurel, A. P., Ghosh, A., Srivastava, V., Giri, B., Seifert, N., and Mendoza, M. M.: Orogenic segmentation and its role in Himalayan mountain building, Front. Earth Sci., 9, 641666, https://doi.org/10.3389/feart.2021.641666, 2021.

Ketcham, R. A.: Forward and inverse modeling of low-temperature thermochronometry data, Rev. Mineral. Geochem., 58, 275–314, https://doi.org/10.2138/rmg.2005.58.11, 2005.

Kirstein, L. A., Fellin, M. G., Willett, S. D., Carter, A., Chen, Y. G., Garver, J. I., and Lee, D. C.: Pliocene onset of rapid exhumation in Taiwan during arc-continent collision: new insights from detrital thermochronometry, Basin Res., 22, 270–285, https://doi.org/10.1111/j.1365-2117.2009.00426.x, 2010.

Kohn, B. P., Gleadow, A. J. W., Brown, R. W., Gallagher, K., O'Sullivan, P. B., and Foster, D. A.: Shaping the Australian crust over the last 300 million years: insights from fission track thermotectonic imaging and denudation studies of key terranes, Austr. J. Earth Sci., 49, 697–717, https://doi.org/10.1046/j.1440-0952.2002.00942.x, 2002.

Lang, K. A., Huntington, K. W., Burmester, R., and Housen, B.: Rapid exhumation of the eastern Himalayan syntaxis since the late Miocene, Geol. Soc. Am. Bull., 128, 1403–1422, https://doi.org/10.1130/b31419.1, 2016.

https://doi.org/10.5194/egusphere-2022-888
Preprint. Discussion started: 7 September 2022

Lang, K. A., Glotzbach, C., Ring, U., Kamp, P. J. J., and Ehlers, T. A.: Linking orogeny and orography in the Southern Alps of New Zealand: New observations from detrital fission-track thermochronology of the Waiho-1 borehole, Earth Planet. Sci. Lett., 552, 116586, https://doi.org/10.1016/j.epsl.2020.116586, 2020.

Mancktelow, N. S. and Grasemann, B.: Time-dependent effects of heat advection and topography on cooling histories during erosion, Tectonophysics, 270, 167–195, https://doi.org/10.1016/s0040-1951(96)00279-x, 1997.

Reiners, P. W. and Brandon, M. T.: Using thermochronology to understand orogenic erosion, Ann. Rev. Earth Planet. Sci., 34, 419–466, https://doi.org/10.1007/978-3-540-48684-8, 2006.

Reiners, P. W., Spell, T. L., Nicolescu, S., and Zanetti, K. A.: Zircon (U-Th)/He thermochronometry: He diffusion and comparisons with $^{40}Ar/^{39}Ar$ dating, Geochim. Cosmochim. Acta, 68, 1857–1887, https://doi.org/10.1016/j.gca.2003.10.021, 2004.

Robert, X., van der Beek, P., Braun, J., Perry, C., Dubille, M., and Mugnier, J. L.: Assessing Quaternary reactivation of the Main Central thrust zone (central Nepal Himalaya): New thermochronologic data and numerical modeling, Geology, 37, 731–734, https://doi.org/10.1130/g25736a.1, 2009.

Schildgen, T. F., van der Beek, P. A., Sinclair, H. D., and Thiede, R. C.: Spatial correlation bias in late-Cenozoic erosion histories derived from thermochronology, Nature, 559, 89–93, https://doi.org/10.1038/s41586-018-0260-6, 2018.

Schildgen, T. F., and van der Beek, P.A.: Thermochronology dataset for Himalaya, Zenodo, https://doi.org/10.5281/zenodo.7053115, 2022.

Stüwe, K., White, L., and Brown, R.: The influence of eroding topography on steady-state isotherms. Application to fission track analysis, Earth Planet. Sci. Lett., 124, 63–74, https://doi.org/10.1016/0012-821x(94)00068-9, 1994.

van der Beek, P.A., and Schildgen, T. F.: age2exhume Matlab scripts, Zenodo, https://doi.org/10.5281/zenodo.7053218, 2022.

van der Beek, P.A., Thiede, R.C., Gahalaut, V.K., and Schildgen, T.F.: Topographic and thermochronologic constraints on the geometry of the Himalayan décollement and its lateral variations, in: Himalaya, Dynamics of a Giant, vol. 1, R. Cattin and J.L. Epard (Eds.), Wiley/ISTE Editions, in press.

Whipp, D. M., Kellett, D. A., Coutand, I., and Ketcham, R. A.: Short communication: Modeling competing effects of cooling rate, grain size, and radiation damage in low-temperature thermochronometers, Geochronol., 4, 143–152, https://doi.org/10.5194/gchron-4-143-2022, 2022.

Willett, S. D. and Brandon, M. T.: Some analytical methods for converting thermochronometric age to erosion rate, Geochem., Geophys., Geosyst., 14, 209–222, https://doi.org/10.1029/2012gc004279, 2013.

Willett, S. D., Herman, F., Fox, M., Stalder, N., Ehlers, T. A., Jiao, R., and Yang, R.: Bias and error in modelling thermochronometric data: resolving a potential increase in Plio-Pleistocene erosion rate, Earth Surf. Dyn., 9, 1153–1221, https://doi.org/10.5194/esurf-9-1153-2021, 2021.

Zeitler, P. K., Meltzer, A. S., Brown, L., Kidd, W. S. F., Lim, C., and Enkelmann, E.: Tectonics and topographic evolution of Namche Barwa and the easternmost Lhasa block, Tibet, Geol. Soc. Am. Spec. Pap., 507, 23–58, https://doi.org/10.1130/2014.2507(02), 2014.